Heliyon 10 (2024) e32888

Contents lists available at ScienceDirect

Heliyon

journal homepage: www.cell.com/heliyon

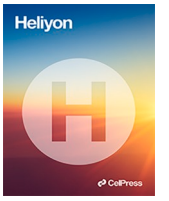

Research article

Structures of SenB and SenA enzymes from *Variovorax paradoxus* provide insights into carbon–selenium bond formation in selenoneine biosynthesis

Sihan Xu [a], Jinyi Zhao [a], Xiang Liu [b], Xiuna Yang [a], Zili Xu [a], Yan Gao [a,**], Yuanyuan Ma [a,*,1], Haitao Yang [a]

[a] *Shanghai Institute for Advanced Immunochemical Studies and School of Life Science and Technology, ShanghaiTech University, Shanghai, 201210, China*

[b] *State Key Laboratory of Medicinal Chemical Biology, Frontiers Science Center for Cell Response, College of Life Sciences, College of Pharmacy, Nankai University, Tianjin, China*

ARTICLE INFO

Keywords:
Selenoneine
Ergothioneine
Carbon–selenium bond
SenB
SenA
Glycosyltransferase
Selenoneine synthase

ABSTRACT

Selenoneine, an ergothioneine analog, is important for antioxidation and detoxification. SenB and SenA are two crucial enzymes that form carbon–selenium bonds in the selenoneine biosynthetic pathway. To investigate their underlying catalytic mechanisms, we obtained complex structures of SenB with its substrate UDP-N-acetylglucosamine (UDP-GlcNAc) and SenA with N-α-trimethyl histidine (TMH). SenB adopts a type-B glycosyltransferase fold. Structural and functional analysis of the interaction network at the active center provide key information on substrate recognition and suggest a metal-ion-independent, inverting mechanism is utilized for SenB-mediated selenoglycoside formation. Moreover, the complex structure of SenA with TMH and enzymatic activity assays highlight vital residues that control substrate binding and specificity. Based on the conserved structure and substrate-binding pocket of the type I sulfoxide synthase EgtB in the ergothioneine biosynthetic pathway, a similar reaction mechanism was proposed for the formation of C–Se bonds by SenA. The structures provide knowledge on selenoneine synthesis and lay groundwork for further applications of this pathway.

1. Introduction

Selenium is an essential trace element across all kingdoms of life. Its antioxidant activity and ability to detoxify mercury play a protective role in many different organisms [1–3]. Selenium derivatives show great potential for altering the potency and selectivity of their original molecules [4]. Ergothioneine, a thiohistidine derivative, is ubiquitously present in most plants and mammals and provides multiple health benefits, such as antioxidative, antiaging and anti-inflammatory effects [5,6]. Few bacteria and non-yeast fungi can synthesize ergothioneine [7,8]. A sulfur-to-selenium substitution in ergothioneine results in the analog selenoneine. Compared to that of ergothioneine, the efficiency by which selenoneine is imported by human cells through highly selective

* Corresponding author.
** Corresponding author.
E-mail addresses: gaoyan@shanghaitech.edu.cn (Y. Gao), mayy2@shanghaitech.edu.cn (Y. Ma).
[1] Lead contact.

https://doi.org/10.1016/j.heliyon.2024.e32888
Received 16 April 2024; Received in revised form 10 June 2024; Accepted 11 June 2024
Available online 14 June 2024
2405-8440/© 2024 Published by Elsevier Ltd. This is an open access article under the CC BY-NC-ND license (http://creativecommons.org/licenses/by-nc-nd/4.0/).

transporters is similar, but selenoneine exhibits a greater reducing effect [9–12].

To date, several ergothioneine biosynthetic pathways, including the *Mycobacterium smegmatis* pathway (EgtA-EgtE) and the fungus *Neurospora crassa* pathway (Egt1/Egt2), have been intensively studied [13,14]. Recently, the selenoneine biosynthetic pathway was discovered, and a widespread three-gene *sen* cassette was found to be responsible for this pathway [15]. SenC, which is encoded in the cluster as a selenophosphate synthetase, catalyzes the first step of this selenometabolite pathway [15]. In addition, SenB (a Se-glycosyltransferase instead of the previously characterized C-, O-, N- and S-glycosyltransferase [16–21]) converts selenophosphate and UDP sugars into selenosugars [15]. Next, SenA, a selenoneine synthase, transfers selenosugars to N-α-trimethyl histidine (TMH) for oxidative C–Se bond formation [15,22,23]. This step is distinct from C–S bond formation in the ergothioneine biosynthetic pathway, in which the sulfoxide synthase type-I EgtB employs γ-glutamyl-cysteine (γ-Glu-Cys), and type-II EgtB and Egt1 use L-cysteine as a sulfur donor [14,23,24] (Fig. 1).

Before the selenoneine biosynthetic pathway was identified, Se-specific metabolic pathways were limited exclusively to the synthesis of selenocysteine and selenouridine by the selenocysteine synthase SelA and the selenouridine synthase SelU, respectively [15,25–27]. In addition to SelA and SelU, SenB and SenA can perform C–Se bond formation. We were interested in the mechanism that underlies these recently reported Se-specific glycosyltransferases SenB and the selenoneine synthase SenA, and we performed structural and functional studies. Here, we obtained the complex structures of SenB, SenA and their substrates. Our structural and functional studies provided vital information regarding selenoneine synthesis and can promote selenoneine production via a synthetic biology approach.

2. Materials and methods

2.1. Expression and purification of SenA, SenB and SenC

Full-length *SenA*, *SenB* and *SenC* in *Variovorax paradoxus* were synthesized (Genewiz) and cloned into pET-28a vector with a small ubiquitin-like modifier (SUMO) tag for promoting solubility and a His-tag at the N-terminus for purification. Various mutants were generated using site-directed mutagenesis. The vector encompassing *SenA*, *SenB*, *SenC* or mutants was individually transformed into *Escherichia coli* BL21(DE3) cells for protein expression. When cells were cultured to mid-log phase (OD_{600} is about 0.8) at 37 °C, 0.08 mM isopropyl β-D-thiogalactoside (IPTG) was added to induce protein expression at 16 °C for 16 h. Then cells were harvested for protein purification at 4 °C. Cell lysis buffer for SenA and SenC purification is consisted of 10 mM Tris-HCl, pH 8.0, 100 mM NaCl, 10 mM imidazole and 10 % (v/v) glycerol, while cell lysis buffer for SenB purification is 25 mM HEPES, pH 7.0, 300 mM NaCl, 10 mM imidazole, 5 % (v/v) glycerol and 1 mM $MgCl_2$. After sonication and spinning down by centrifugation, supernatants were loaded onto a Ni-NTA column. Contaminants were sequentially washed with lysis buffer plus 20 mM and 50 mM imidazole. Later, the N-terminal

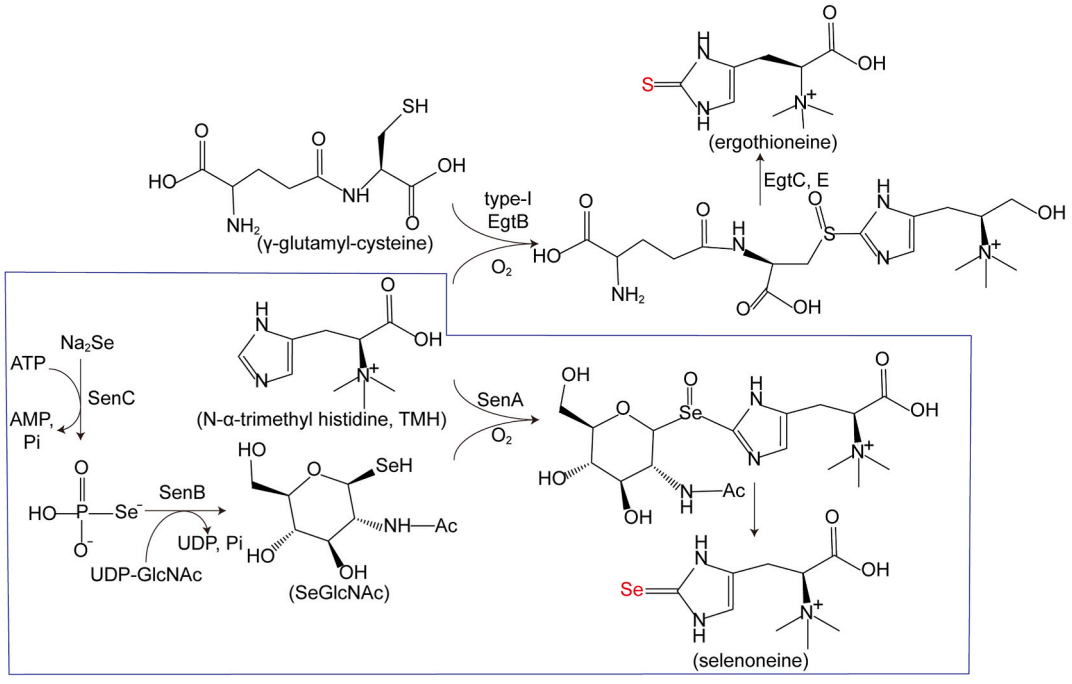

Fig. 1. Key steps in the ergothioneine and selenoneine biosynthetic pathways. Top, C–S bond formation catalyzed by type-I EgtB in *Mycobacterium smegmatis*. Bottom, C–Se bond formation by SenB and SenA. The difference between ergothioneine and selenoneine is labeled in red. (For interpretation of the references to color in this figure legend, the reader is referred to the Web version of this article.)

SUMO tag of SenA, SenB and SenC was removed by protease Ulp1 overnight on beads. The elute of SenA was collected for further purification by size exclusion chromatography Superdex 75 Increase 10/300 GL (Cytiva), the elute of SenB was purified by ion-exchange column HiTrap SP HP 5 mL (Cytiva) and Superdex 75 Increase 10/300 GL, whereas the elute of SenC was purified by ion-exchange column HiTrap Q HP 5 mL (Cytiva) and Superdex 200 Increase 10/300 GL. The purified SenA, SenB and SenC were collected and concentrated for crystallization and activity assays.

2.2. Crystallization, data collection and structure determination

SenA, at a concentration of 15 mg mL^{-1}, was incubated with N-α-trimethyl histidine (TMH) at a molar ratio of 1:10 for 30 min at 4 °C, and then the binary complex was set up tray for crystallization screen by hanging drop method at a volume ratio of 1:2 (SenA: well buffer) at 20 °C. The best crystals grew in crystallization buffer containing 0.64 M potassium sodium tartrate, 0.08 M CHES sodium pH 9.5, 1.6 M lithium sulfate monohydrate, 0.5 M NaCl and 10 % (w/v) PEG 6000. After a week, crystals were harvested using crystallization buffer plus 20 % (v/v) glycerol as a cryoprotectant, flash-cooled, and stored in liquid nitrogen for data collection.

SenB, at a concentration of 15 mg mL^{-1}, was incubated with UDP-GlcNAc at a molar ratio of 1:10 for 30 min at 4 °C, and then crystallization conditions were screened by sitting drop vapor diffusion method at 20 °C. The best crystals grew in buffer containing 50 mM magnesium sulfate hydrate, 50 mM HEPES sodium pH 7.0, and 1.6 M lithium sulfate monohydrate. Crystals were harvested and flash-cooled using crystallization buffer plus 20 % (v/v) glycerol as a cryoprotectant for data collection.

X-ray diffraction data of SenA and SenB were collected on beamlines BL17U1 and BL19U1 at Shanghai Synchrotron Radiation Facility (SSRF) at a wavelength of 0.978530 Å and 0.979183 Å, respectively. 360 frames were collected with oscillation angle of 1° per frame for each set of data. Data integration and scaling were performed using program XDS [28]. Molecular replacement, using the program PHASER [29], was utilized for structure determination of SenA and SenB by using AlphaFold models of an ergothioneine biosynthesis protein EgtB (UniProt access number T1XAV7) and a glycosyltransferase (UniProt access number T1XAF6) in *Variovorax paradoxus* B4 as search models, respectively. Ligand structures and geometric constraints were generated by phenix.elbow program [30]. Then the output models were subsequently subjected to iterative cycles of model adjustment using Coot and refinement using Phenix [31,32]. Finally, all the residues are located in the allowed region of Ramachandran Plot for structure of SenA, while 0.63 % residues of SenB in disallowed regions. The data collection and structure refinement statistics are summarized in Table 1.

2.3. SenA activity assays

In order to remove nickel ion at the active site, 20 mM EDTA was added and incubated with SenA on ice for 30 min, and then removed by size exclusion chromatography. Using the EDTA-treated SenA, 100-μL reactions were prepared as previously reported [15], containing 50 mM Tris-HCl, 150 mM NaCl, pH 8.0, 1 mM DTT, 1 mM N-α-trimethyl histidine, 1 mM synthetic dimeric SeGlcNAc (Shanghai Medicilon Inc.), 20 μM SenA, and 0.2 mM $(NH_4)_2Fe(SO_4)_2$. For EDTA-untreated SenA, $(NH_4)_2Fe(SO_4)_2$ was not included in

Table 1
Data collection and refinement statistics.

	SenB-UDP-GlcNAc (PDB-8RZ3)	SenA-TMH (PDB-8RYZ)
Data collection		
Space group	$P12_11$	$P3_121$
Cell dimensions		
a, *b*, *c* (Å)	107.90, 56.32, 108.05	118.00, 118.00, 72.80
α, β, γ (°)	90.00, 90.94, 90.00	90.00, 90.00, 120.00
Resolution (Å)	49.87-2.15 (2.23-2.15)[a]	45.84-2.02 (2.09-2.02)
R_{merge}	0.15 (0.96)	0.11 (1.23)
$I/\sigma(I)$	8.20 (1.70)	18.30 (1.60)
Completeness (%)	99.90 (99.99)	99.86 (98.5)
Redundancy	6.30 (5.23)	18.40 (11.11)
Wilson B factors ($Å^2$)	47.44	35.25
Refinement		
Resolution range (Å)	48.62-2.15	34.29-2.02
No. of reflections	71,180	38,568
R_{work}/R_{free} (%)	23.67/28.56	18.02/21.69
No. atoms		
Protein	7264	3219
Ligand/ion	117	57
Water	180	223
Average *B*-factors ($Å^2$)	46.85	36.48
Protein	46.78	36.69
Ligand/ion	48.80	36.34
Water	48.39	33.53
R.m.s. deviations		
Bond lengths (Å)	0.010	0.008
Bond angles (°)	1.14	0.91

[a] Values in parentheses are for the highest-resolution shell.

the reaction system. Both reactions were incubated at room temperature for 120 min. Then one-tenth volume of mBBr (3 μg μL^{-1}) was added and incubated for 30 min to allow for complete derivatization with mBBr. Finally, HPLC–MS using an ACE-C4 column (100 mm × 2.1 mm, 5 μm) at 75 °C was employed for product analysis. HPLC–MS was performed on an AB SCIEX QTOF4600 mass spectrometer equipped with a Shimadzu 30A HPLC, an automated liquid sampler, and AB SCIEX 4600 ESI source. 5 μL samples were loaded each time. Solvent A for HPLC–MS experiments was water and 0.1 % formic acid, and solvent B was acetonitrile and 0.1 % formic acid. Gradient: 0 min 5 %, 0–3.5 min 15 %, 3.5–5 min 15–95 %, 5–6.5 min 95 %, 6.5–8 min 95-5% B at flow rate of 0.4 mL min^{-1}. HPLC–MS data were acquired, analyzed with PEAKS software and figure generated by Excel. Activity assays of SenA mutants were performed the same as EDTA-treated SenA.

2.4. Structural characterization of SenA products

For structural characterization of SenA products, a 10-mL SenA enzymatic assay was carried out as described above. SEN–mBBr was purified as follows. HPLC was performed on Waters 2545 machine, using an Sunfire Prep C18 column (19 × 250 mm, 5 μm). Solvent A

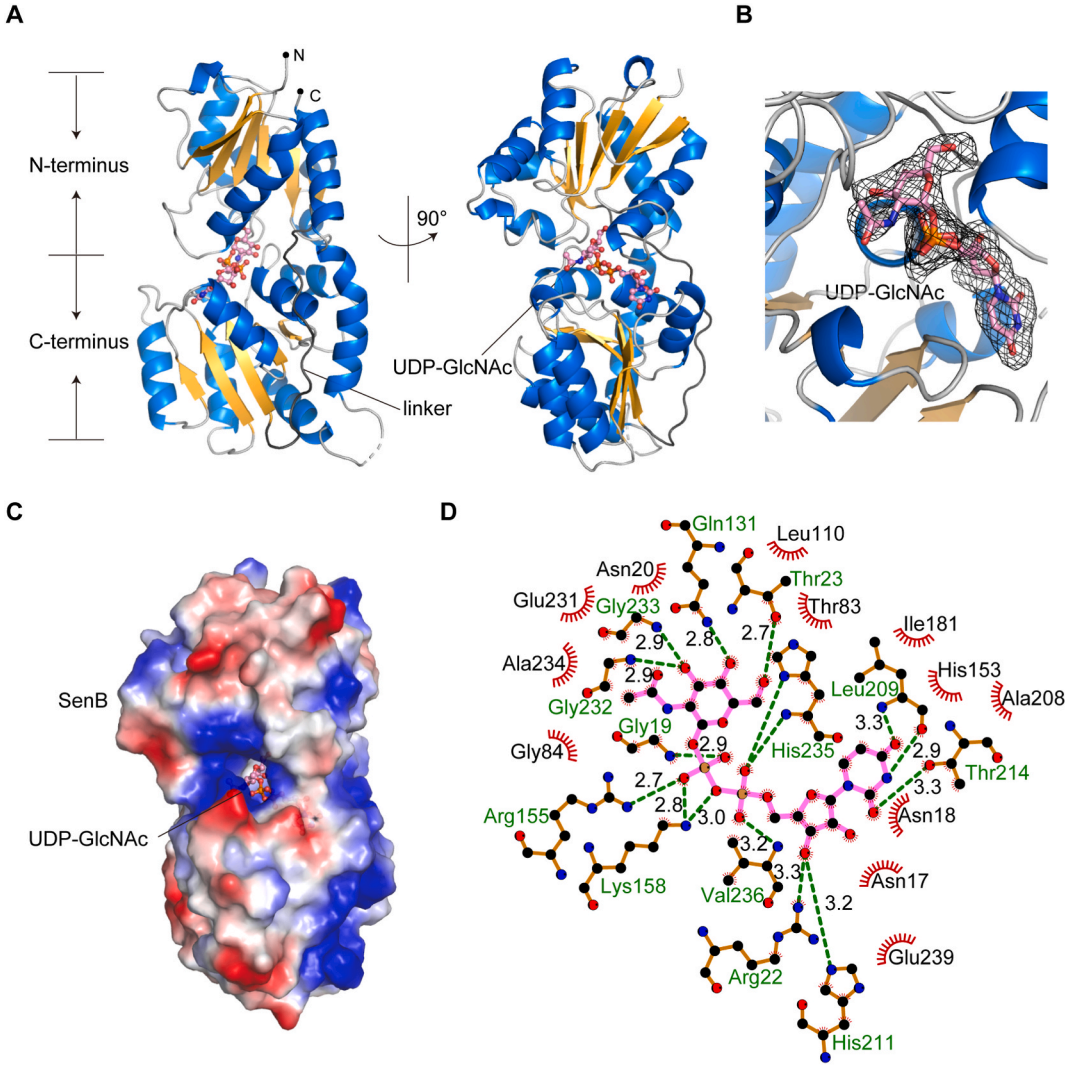

Fig. 2. Structural analysis of the glycosyltransferase SenB in complex with UDP-GlcNAc. (A) Overall structure of the SenB-UDP-GlcNAc binary complex in two vertical views. SenB and the ligand UDP-GlcNAc are shown as cartoons and spheres, respectively. α-helices are colored marine, β-sheets light-orange, loops light-gray while linker between N- and C-terminus dark-gray. The N- and C-termini of SenB are labeled with black dots. **(B)** The mFo-DFc omit map for the ligand UDP-GlcNAc was constructed at σ-level = 2.0 (black mesh). **(C)** Electrostatic potential map showing the substrate-binding pocket. **(D)** The interaction network of the ligand UDP-GlcNAc with SenB. The hydrogen bonds formed for the stabilization of UDP-GlcNAc are shown as green dashed lines. The residue names for hydrogen bond formation and the distance between hydrogen bonds are shown in green and black, respectively. The unit of the hydrogen bond length is angstroms (Å). (For interpretation of the references to color in this figure legend, the reader is referred to the Web version of this article.)

for HPLC experiments was 0.05 % (v/v) HCl in H_2O and solvent B was acetonitrile. Gradient: 0–1 min 5 %, 1–25 min 5–25 % B, 25–28 min 25–100 % B, 28–30 min 100 % B at flow rate of 2.5 mL min^{-1}; detector: UV detection (λ_{max} = 220–254 nm). NMR spectra were recorded on a Bruker-600 (600 MHz) instrument. The deuterated solvents employed were purchased from Energy Chemical. Chemical shifts were given in ppm with respect to referenced solvent peaks. Spectra were analyzed with MestReNova.

2.5. SenB activity assays

100-μL reactions were prepared under anaerobic conditions as previously reported [15], containing 50 mM Tris, pH 7.2, 20 mM KCl, 5 mM $MgCl_2$, 2 mM DTT, 2 mM ATP, 1 mM Na_2Se, 2 mM UDP-GlcNAc, 20 μM SenC and 20 μM SenB. After a 6-h incubation period at room temperature, reactions were removed from the glovebox and exposed to oxygen for 30 min to oxidize any unreacted Na_2Se. Then, one-fifth volume of 10 mM mBBr in MeCN was added and incubated for an additional 30 min in the dark to allow for complete derivatization with mBBr. After centrifugation at 12,000×*g* for 30 min, the supernatants were collected and analyzed at a single wavelength of 390 nm on Agilent 1290 infinity II LC system with a ZORBAX SB-C18 column (100 mm × 2.1 mm, 1.8 μm) at 50 °C. 10 μL samples were loaded each time. Solvent A for HPLC system was water and 0.1 % trifluoroacetic acid, and solvent B was acetonitrile and 0.1 % trifluoroacetic acid. Gradient: 0–0.5 min 10 %, 0.5–12.5 min 10–22 %, 12.5–15 min 22–50 %, 15–16 min 50–100 % B at flow rate of 0.6 mL min^{-1}.

3. Results and discussion

3.1. Overall structure of SenB

The recombinant protein SenB was expressed in *Escherichia coli* BL21 (DE3) and processed to generate a monomer with high purity and homogeneity (Supplementary Fig. S1). For crystallization, the SenB protein was incubated with the substrate nucleotide sugar UDP-N-acetylglucosamine (UDP-GlcNAc) at a molar ratio of 1:10. The crystal structure of the SenB-UDP-GlcNAc binary complex was refined at a resolution of 2.15 Å, containing three copies of SenB in an asymmetric unit. Three SenB molecules strongly resembled each other after superimposition, with a Cα root mean square (r.m.s.) deviation of 0.42 Å between monomers A and B, 0.68 Å between monomers A and C and 0.55 Å between monomers B and C. Based on the best electron density, the structure of monomer C was built and chosen for further structural analysis. The data collection and refinement statistics are summarized in Table 1.

The whole chain of SenB is well defined except for C-terminal residues 328–331, for local flexibility (Fig. 2 panel A). The architecture of SenB consists of two domains that were connected by a long hinge loop (residues 131–146) (Fig. 2 panel A). The N- (residues 1–130) and C-terminal (residues 147–331) domains exhibited β/α/β Rossmann-like folds (Fig. 2 panel A). The two domains face each other and are less tightly associated, which is a typical domain arrangement of the glycosyltransferase GT-B fold superfamily [21]. The last helix at the C-terminal domain crosses back and associates with the N-terminal domain (Fig. 2 panel A).

3.2. Donor substrate binding of SenB

The active sites of SenB lie within a cleft between the N- and C-domains, in which no metal ions are present and the sugar donor UDP-GlcNAc fits well according to the electron density map (Fig. 2 panels A and B). The residues form a positively charged substrate binding pocket, accommodating the negatively charged sugar acceptor selenophosphate (SeP) (Fig. 2 panel C). The GlcNAc moiety at the sugar donor binds in a "bent back" manner relative to the pyrophosphate moiety of UDP (Fig. 2 panel B). The uracil base of UDP forms hydrogen bonds with the main chain of Leu209 and the hydroxyl group of Thr214 and the ribose hydrogen bonds with the side chains of Arg22 and His211 (Fig. 2 panel D). Metal-dependent GT-A fold glycosyltransferases utilize a coordinated divalent cation for stabilizing nucleoside diphosphate leaving groups [21,33,34]; in contrast, SenB employs the main chain amides Gly19, His235 and Val236 and the positively charged side chains Arg155 and Lys158 to neutralize the negative charges of the α- and β-phosphoryl groups and facilitate their departure (Fig. 2 panel D). The GlcNAc moiety is tightly bound to the active sites by hydrogen bonding with residues Thr23, Gln131, Glu232 and Gly233 of SenB (Fig. 2 panel D). Analysis of the sugar donor interaction network demonstrated that, except for the first helix (residues 19–34) in the N-terminal domain, the main anchoring interactions of UDP-GlcNAc originated from the C-terminal domain (Fig. 2 panel D).

3.3. Proposed catalytic mechanism of SenB

To explore the possible sugar transfer mechanism, the sugar acceptor selenophosphate was docked into the structure of SenB (Supplementary Fig. S2 panel A) [35,36]. Selenophosphate lies in a size- and charge-complementary groove over UDP-GlcNAc and is within hydrogen-bonding distance (3.1 Å) to one oxygen in β-phosphate (Supplementary Fig. S2). The side chains of Asn20, His58, Thr83 and Arg155 and the main chain of Gly84 are situated within the hydrogen bonding distance of selenophosphate and therefore likely recognize and orient the incoming acceptor (Supplementary Fig. S2 panel B). This spatial arrangement renders SenB to adopt an inverting reaction mechanism in which nucleophilic attack at the sugar anomeric C1 and UDP removal occur on opposite faces (Supplementary Fig. S2 panel B). This is in line with generation of product 1-Se-β-D-glucose from substrate UDP-α-D-glucose by SenB [15]. For Se–P bond cleavage, specific lysine residues are utilized by bacterial SelA and human SepSecS in selenocysteine formation [37,38]. Here in SenB, Lys158 is the most suitably positioned candidate for breaking the Se–P bond (Fig. 2 panel D; Supplementary Fig. S2 panel B). To corroborate our structural analysis, we employed enzymatic activity assays to examine activity changes caused by

the missense mutations at the active center of SenB. Individual alanine substitution of the residues possibly disrupting selenophosphate binding (N20A, H58A, T83A and R155A) displayed minor decreases in activity of SenB (Supplementary Fig. S2 panels C and D). By contrast, replacement of residue lysine l58 to alanine (K158A) greatly impaired the activity of SenB, indicating that Lys158 is a potential catalytic residue of SenB (Supplementary Fig. S2 panels C and D). Together, we speculate that SenB utilizes Lys158 as a catalytic residue to generate selenosugars as a metal ion-independent, inverting glycosyltransferase (Fig. 2; Supplementary Fig. S2).

Recent work reported structures of SenB in apo form and in UDP-Glc/PO_4^{3-} binding form [39,40]. Unexpectedly, structural comparison of SenB in different states merely displayed local conformational changes, distinct from some other GT-B enzymes showing large substrate-induced conformational changes (Supplementary Fig. S3) [35,39–42]. The minor ligand-induced shift in the overall structure indicates that the obvious diameter decrease upon substrate binding measured by SAXS is inappropriate [39]. Selenophosphate sugar intermediates were detected, indicating that a ternary complex of SenB and SeP/Glc forms before Se–P bond breakage [40]. In our structural study, substrate UDP-GlcNAc was not catalyzed into product UDP when selenophosphate was not included in the reaction system. Therefore, SenB probably generates selenosugars in a sequential manner. Further investigations are needed for the kinetic mechanism study of SenB.

3.4. Overall structure of SenA

SeGlcNAc, the product of the glycosyl transfer reaction catalyzed by the selenosugar synthase SenB, is the preferred substrate of the selenoneine synthase SenA (Fig. 1) [15]. Next, we purified SenA and explored its catalytic mechanism.

The recombinant protein SenA was expressed in *Escherichia coli* BL21 (DE3) and sequentially purified with a Ni-NTA affinity column and size-exclusion chromatography (Supplementary Fig. S1 panels D and E). The crystal structure of the SenA and N-

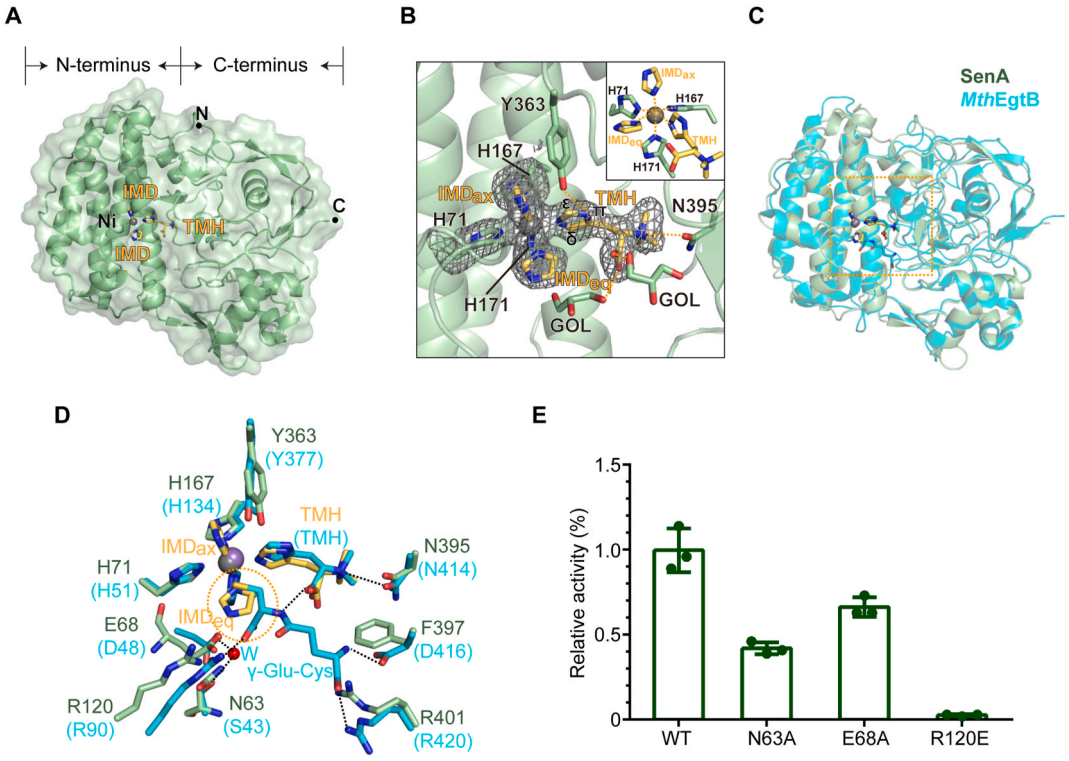

Fig. 3. Structural analysis of the selenoneine synthase SenA in complex with TMH. (A) Overall structure of the SenA-TMH complex. The N- and C-terminal domains of SenA are shown as pale-green cartoons and surfaces, the ligand TMH and two imidazoles are shown as yellow sticks, and nickel ions are shown as gray spheres. The N- and C-termini are marked with black dots. **(B)** The mFo-DFc omit map of the coordination site contoured at 2σ (gray mesh). Residues and ligands are shown in the same color as in panel (A). Inset, the other view showing the coordination sites. GOL indicates the glycerol observed in the structure. Hydrogen bonds are shown as yellow-orange dashed lines. **(C)** Structural alignment between SenA and *Mth*EgtB. SenA and its ligands are shown as in panel (A), while *Mth*EgtB and its substrates TMH and γ-Glu-Cys and manganese ions are shown as cyan cartoons, cyan sticks and purple spheres, respectively. The substrate-binding pocket is shown in the yellow-orange dashed box and is enlarged for analysis in panel (D). **(D)** Comparison of the substrate binding pockets between SenA and *Mth*EgtB. Residues and ligands of *Mth*EgtB and SenA are shown in the same colors as those in panel (C). The dashed orange oval indicates the possible binding volume for the selenosugar substrate SenA. Water molecules are shown as red spheres and labeled with the letter W. **(E)** Relative catalytic activities of the SenA mutants. The data were quantified from three replicates with average and SD shown. (For interpretation of the references to color in this figure legend, the reader is referred to the Web version of this article.)

α-trimethyl histidine (TMH) binary complex was determined at a resolution of 2.02 Å and contained one copy of the protein in an asymmetric unit. In addition to the flexible N- and C-termini (residues 1–6, 415–416) and the linker (residues 190–192) between the N- and C-terminal domains, the whole chain can be traced, and the model was constructed (Fig. 3 panel A). The data collection and refinement statistics are summarized in Table 1.

SenA is composed of an N-terminal helical domain (residues 1 to 189) and a C-terminal domain (residues 190 to 416) that consists of an α-ββ-α fold (Fig. 3 panel A). The active sites of SenA are located at the interface between the N- and C-terminal domains (Fig. 3 panel A). A Dali search revealed that SenA is structurally similar to *Mycolicibacterium thermoresistibile* sulfoxide synthase EgtB (*Mth*EgtB) (PDB-4X8D), with a r.m.s. deviation of 1.9 Å and a Z score of 41.2 (Supplementary Fig. S4) [43]. A striking difference from *Mth*EgtB is that SenA contains a longer N-terminus, which harbors a loop and a helix (approximately 23 residues) (Supplementary Fig. S4).

3.5. Catalytic center and analysis of the substrate specificity of SenA

At the coordination site, a conserved three-His facial triad (His71, His167, His171) and the ligand TMH were involved in metal ion binding (Fig. 3 panels A and B). Using inductively coupled plasma–mass spectrometry (ICP–MS), we determined that most metal ions coordinated here were nickel ions instead of iron ions, probably due to the protein affinity of SenA purified by a Ni-NTA column. Further density refinement demonstrated that the other two ligands coordinating the metal ion are imidazole molecules (Fig. 3 panels A and B) in place of solvent water or anions in other sulfoxide synthases [22,23]. We defined the imidazole opposite to His167 as the equatorial imidazole (IMD_{eq}) and the other opposite to His171 as the axial imidazole (IMD_{ax}) (Fig. 3 panel B). Further enzymatic assays involving high-performance liquid chromatography–mass spectrometry (HPLC–MS) showed that the purified SenA with nickel ions was inactive (Supplementary Fig. S5), whereas SenA treated with EDTA, followed by EDTA removal and the addition of $(NH_4)_2Fe(SO_4)_2$, retained strong activity (Supplementary Figs. S5 and S6), corresponding with previous results that SenA is a nonheme iron-dependent enzyme [15]. Structural analysis suggested that the catalytic residue of SenA is Tyr363 at the C-terminal domain (Fig. 3 panel B). A C–Se bond is formed at the imidazole ε-position rather than at the δ-position, similar to most sulfoxide synthase EgtB in the EGT pathway [22,23,44]. In addition to interacting with metal ions, the substrate TMH can form hydrogen bonds with the hydroxyl group of Tyr363 and the side chain amide group of Asn395 via its imidazole π-nitrogen and trimethylated amino group, respectively (Fig. 3 panel B). Moreover, two solvent glycerol molecules were observed to interact with TMH via their carboxyl groups (Fig. 3 panel B).

Due to the dimerization of the preferred substrate SeGlcNAc of SenA, we utilized the analog GlcNAc and expected to generate a trinary complex containing SenA, TMH and GlcNAc. Unfortunately, we were unable to generate crystals of SenA with GlcNAc despite an extensive search for appropriate cocrystallization and soaking conditions. As an alternative, we explored the catalytic mechanism of SenA through structural alignment with the previously reported homologous structure of *Mth*EgtB and the substrates TMH and γ-Glu-Cys (PDB-4X8D), in which γ-Glu-Cys is a direct ligand for the catalytic metal ion and occupies the position of the equatorial ion at the coordination sites (Fig. 3 panels C and D). Similarly, the sugar donor SeGlcNAc at SenA may substitute the equatorial ligand to approach the imidazole moiety of TMH for catalysis (Fig. 3 panel D). The substrate-binding pockets of SenA and *Mth*EgtB exhibited remarkable similarities except for two changes (Fig. 3 panel D). The first change is residue substitution. Asp416 in *Mth*EgtB, which forms hydrogen bonds with the glutamyl moiety of γ-Glu-Cys, is replaced by the hydrophobic residue Phe397 in SenA (Fig. 3 panel D). The second factor is residue conformation change. Compared with residue Arg420 in *Mth*EgtB, the side chain conformation of corresponding conserved residue Arg401 in SenA was significantly different (Fig. 3 panel D). This leads to a steric clash with the glutamyl moiety if the substrate of SenA is γ-Glu-Cys (Fig. 3 panel D). The mutation and conformation changes observed here provide an explanation for the difference in substrate specificity between *Mth*EgtB and SenA (Fig. 3 panel D). On the other hand, the residues Arg90, Asp48 and Ser43 in *Mth*EgtB form hydrogen bonds with the cysteinyl moiety of γ-Glu-Cys directly or in a water-mediated manner to stabilize *Mth*EgtB, whereas the corresponding residues in SenA are Arg120, Glu68 and Asn63 (Fig. 3 panel D). Sequence and structure comparisons indicated that these three residues likely play critical roles in the binding of substrate SeGlcNAc to SenA (Fig. 3 panel D). In accordance with our structural analysis, replacement of individual residue to alanine at the substrate binding pocket (N63A and E68A) greatly impaired the catalytic activity of sulfoxide synthase SenA (Fig. 3 panel E; Supplementary Fig. 7). Moreover, individual mutation to the opposite charge residue (R120E) completely abolished the catalytic activity of SenA, indicating that the residue Arg120 is essential for substrate SeGlcNAc binding (Fig. 3 panel E; Supplementary Fig. 7). This is consistent with a recently published structure of SenA which shows the binding mode of these three residues with substrates [45]. Next, we discuss the mechanism of C–Se bond formation catalyzed by SenA.

3.6. A proposed catalytic mechanism of SenA

SenA is a nonheme iron-dependent enzyme that requires O_2 for activity [15]. Increasing evidence shows that these enzymes form Fe(III)-superoxide complexes by simple addition of O_2 to the reduced [Fe(II)] for the initiation of substrate oxidation [46–48]. Previously reported catalytic process of the sulfoxide synthase *Mth*EgtB, the structural homolog of SenA, on the basis of the use of its trinary complex with N-α-dimethyl histidine (DMH) and γ-Glu-Cys and the identification of the S-stent configuration of its sulfoxide product [23,49]. Here, we refer to the reaction mechanism of *Mth*EgtB and propose the putative subsequent steps of SenA (Supplementary Fig. 8). After the reduced [Fe(II)] was oxidized, the catalytic residue Tyr363 transfers a proton to reduce the iron:oxygen complex, the iron(III)-complexed selenium analog of the thiyl radical attacks the imidazole ring of TMH and a C–Se bond is formed [23,49]. Next, electrons are transferred to Fe(III), and selenoxide compounds are generated [23,50]. However, further investigations are needed to

explore the stereochemistry of the product of SenA and its detailed catalytic mechanism.

In conclusion, we solved the crystal structures of the glycosyltransferase SenB and the selenoneine synthase SenA, two enzymes specific for selenoneine biosynthesis. Analysis of the structures of SenB and SenA with their ligands and functional data provide key information on substrate recognition and extends our knowledge on the biosynthesis pathway of selenometabolites. The structures of SenB and SenA reported here and structural comparisons with their homologous enzymes allowed us to propose and discuss the possible catalytic mechanisms of these two enzymes. Moreover, investigations of SenB and SenA could expand knowledge on the biosynthesis pathway of the popular molecule ergothioneine.

4. Funding statement

This work was supported by grants from the National Natural Science Foundation of China (grant no. 32394010 to Z.H.R.); the National Key R&D Program of China (grant no. 2022YFC2302900 to H.T.Y.); and the Shanghai Frontiers Science Center for Biomacromolecules and Precision Medicine of ShanghaiTech University.

5. data availability statement

The atomic coordinates in this study have been deposited in the Protein Data Bank with the accession codes 8RZ3 (SenB-UDP-GlcNAc complex) and 8RYZ (SenA-TMH complex).

CRediT authorship contribution statement

Sihan Xu: Methodology. **Jinyi Zhao:** Methodology. **Xiang Liu:** Validation, Software. **Xiuna Yang:** Methodology. **Zili Xu:** Methodology. **Yan Gao:** Validation, Software. **Yuanyuan Ma:** Writing – review & editing, Writing – original draft, Validation, Software, Methodology, Investigation, Data curation, Conceptualization. **Haitao Yang:** Investigation, Funding acquisition, Data curation, Conceptualization.

Declaration of competing interest

The authors declare that they have no known competing financial interests or personal relationships that could have appeared to influence the work reported in this paper.

Acknowledgments

We thank the staff from beamlines BL17U1 and BL19U1 at the Shanghai Synchrotron Radiation Facility (SSRF) and the SIAIS Analytical Chemistry Platform at ShanghaiTech University for providing technical support and assistance during the data collection.

Appendix A. Supplementary data

Supplementary data to this article can be found online at https://doi.org/10.1016/j.heliyon.2024.e32888.

References

[1] M.L. Cuvin-Aralar, R.W. Furness, Mercury and selenium interaction: a review, Ecotoxicol. Environ. Saf. 21 (1991) 348–364, https://doi.org/10.1016/0147-6513(91)90074-y.
[2] J. Fleming, A. Ghose, P.R. Harrison, Molecular mechanisms of cancer prevention by selenium compounds, Nutr. Cancer 40 (2001) 42–49, https://doi.org/10.1207/s15327914nc401_9.
[3] L. Kiremidjian-Schumacher, M. Roy, Effect of selenium on the immunocompetence of patients with head and neck cancer and on adoptive immunotherapy of early and established lesions, Biofactors 14 (2001) 161–168, https://doi.org/10.1002/biof.5520140121.
[4] W. Hou, H. Dong, X. Zhang, Y. Wang, L. Su, H. Xu, Selenium as an emerging versatile player in heterocycles and natural products modification, Drug Discov. Today 27 (2022) 2268–2277, https://doi.org/10.1016/j.drudis.2022.03.020.
[5] I.K. Cheah, B. Halliwell, Ergothioneine; antioxidant potential, physiological function and role in disease, Biochim. Biophys. Acta 1822 (2012) 784–793, https://doi.org/10.1016/j.bbadis.2011.09.017.
[6] L. Chen, L. Zhang, X. Ye, Z. Deng, C. Zhao, Ergothioneine and its congeners: anti-ageing mechanisms and pharmacophore biosynthesis, Protein Cell (2023), https://doi.org/10.1093/procel/pwad048, 10.1093/procel/pwad048.
[7] D.S. Genghof, O. Vandamme, Biosynthesis of ergothioneine and hercynine by mycobacteria, J. Bacteriol. 87 (1964) 852–862, https://doi.org/10.1128/jb.87.4.852-862.1964.
[8] C. Pfeiffer, T. Bauer, B. Surek, E. Schömig, D. Gründemann, Cyanobacteria produce high levels of ergothioneine, Food Chem. 129 (2011) 1766–1769, https://doi.org/10.1016/j.foodchem.2011.06.047.
[9] Y. Yamashita, M. Yamashita, Identification of a novel selenium-containing compound, selenoneine, as the predominant chemical form of organic selenium in the blood of bluefin tuna, J. Biol. Chem. 285 (2010) 18134–18138, https://doi.org/10.1074/jbc.C110.106377.
[10] D. Lim, D. Gründemann, F.P. Seebeck, Total synthesis and functional characterization of selenoneine, Angew Chem. Int. Ed. Engl. 58 (2019) 15026–15030, https://doi.org/10.1002/anie.201908967.

[11] D. Gründemann, S. Harlfinger, S. Golz, A. Geerts, A. Lazar, R. Berkels, N. Jung, A. Rubbert, E. Schömig, Discovery of the ergothioneine transporter, Proc. Natl. Acad. Sci. U.S.A. 102 (2005) 5256–5261, https://doi.org/10.1073/pnas.0408624102.

[12] D.G. Dumitrescu, E.M. Gordon, Y. Kovalyova, A.B. Seminara, B. Duncan-Lowey, E.R. Forster, W. Zhou, C.J. Booth, A. Shen, P.J. Kranzusch, S.K. Hatzios, A microbial transporter of the dietary antioxidant ergothioneine, Cell 185 (2022) 4526–4540.e4518, https://doi.org/10.1016/j.cell.2022.10.008.

[13] F.P. Seebeck, In vitro reconstitution of Mycobacterial ergothioneine biosynthesis, J. Am. Chem. Soc. 132 (2010) 6632–6633, https://doi.org/10.1021/ja101721e.

[14] W. Hu, H. Song, A. Sae Her, D.W. Bak, N. Naowarojna, S.J. Elliott, L. Qin, X. Chen, P. Liu, Bioinformatic and biochemical characterizations of C–S bond formation and cleavage enzymes in the fungus Neurospora crassa ergothioneine biosynthetic pathway, Org. Lett. 16 (2014) 5382–5385, https://doi.org/10.1021/ol502596z.

[15] C.M. Kayrouz, J. Huang, N. Hauser, M.R. Seyedsayamdost, Biosynthesis of selenium-containing small molecules in diverse microorganisms, Nature 610 (2022) 199–204, https://doi.org/10.1038/s41586-022-05174-2.

[16] D. Teze, J. Coines, F. Fredslund, K.D. Dubey, G.N. Bidart, P.D. Adams, J.E. Dueber, B. Svensson, C. Rovira, D.H. Welner, *O-/N-/S*-Specificity in glycosyltransferase catalysis: from mechanistic understanding to engineering, ACS Catal. 11 (2021) 1810–1815, https://doi.org/10.1021/acscatal.0c04171.

[17] M. Brazier-Hicks, W.A. Offen, M.C. Gershater, T.J. Revett, E.K. Lim, D.J. Bowles, G.J. Davies, R. Edwards, Characterization and engineering of the bifunctional N- and O-glucosyltransferase involved in xenobiotic metabolism in plants, Proc. Natl. Acad. Sci. U.S.A. 104 (2007) 20238–20243, https://doi.org/10.1073/pnas.0706421104.

[18] J. Ati, P. Lafite, R. Daniellou, Enzymatic synthesis of glycosides: from natural O- and N-glycosides to rare C- and S-glycosides, Beilstein J. Org. Chem. 13 (2017) 1857–1865, https://doi.org/10.3762/bjoc.13.180.

[19] D.M. Liang, J.H. Liu, H. Wu, B.B. Wang, H.J. Zhu, J.J. Qiao, Glycosyltransferases: mechanisms and applications in natural product development, Chem. Soc. Rev. 44 (2015) 8350–8374, https://doi.org/10.1039/c5cs00600g.

[20] K. Xie, R. Chen, J. Li, R. Wang, D. Chen, X. Dou, J. Dai, Exploring the catalytic promiscuity of a new glycosyltransferase from *Carthamus tinctorius*, Org. Lett. 16 (2014) 4874–4877, https://doi.org/10.1021/ol502380p.

[21] L.L. Lairson, B. Henrissat, G.J. Davies, S.G. Withers, Glycosyltransferases: structures, functions, and mechanisms, Annu. Rev. Biochem. 77 (2008) 521–555, https://doi.org/10.1146/annurev.biochem.76.061005.092322.

[22] N. Naowarojna, S. Irani, W. Hu, R. Cheng, L. Zhang, X. Li, J. Chen, Y.J. Zhang, P. Liu, Crystal structure of the ergothioneine sulfoxide synthase from *Candidatus Chloracidobacterium thermophilum* and structure-guided engineering to modulate its substrate selectivity, ACS Catal. 9 (2019) 6955–6961, https://doi.org/10.1021/acscatal.9b02054.

[23] K.V. Goncharenko, A. Vit, W. Blankenfeldt, F.P. Seebeck, Structure of the sulfoxide synthase EgtB from the ergothioneine biosynthetic pathway, Angew Chem. Int. Ed. Engl. 54 (2015) 2821–2824, https://doi.org/10.1002/anie.201410045.

[24] A.S. Faponle, F.P. Seebeck, S.P. de Visser, Sulfoxide synthase versus cysteine dioxygenase reactivity in a nonheme iron enzyme, J. Am. Chem. Soc. 139 (2017) 9259–9270, https://doi.org/10.1021/jacs.7b04251.

[25] J.T. Rotruck, A.L. Pope, H.E. Ganther, A.B. Swanson, D.G. Hafeman, W.G. Hoekstra, Selenium: biochemical role as a component of glutathione peroxidase, Science 179 (1973) 588–590, https://doi.org/10.1126/science.179.4073.588.

[26] L. Zhong, A. Holmgren, Essential role of selenium in the catalytic activities of mammalian thioredoxin reductase revealed by characterization of recombinant enzymes with selenocysteine mutations, J. Biol. Chem. 275 (2000) 18121–18128, https://doi.org/10.1074/jbc.M000690200.

[27] A.J. Wittwer, L. Tsai, W.M. Ching, T.C. Stadtman, Identification and synthesis of a naturally occurring selenonucleoside in bacterial tRNAs: 5-[(methylamino) methyl]-2-selenouridine, Biochemistry 23 (1984) 4650–4655, https://doi.org/10.1021/bi00315a021.

[28] W. Kabsch, Xds, Acta Crystallogr. D 66 (2010) 125–132, https://doi.org/10.1107/S0907444909047337.

[29] A.J. Mccoy, R.W. Grosse-Kunstleve, P.D. Adams, M.D. Winn, L.C. Storoni, R.J. Read, Phaser crystallographic software, J. Appl. Crystallogr. 40 (2007) 658–674, https://doi.org/10.1107/S0021889807021206.

[30] N.W. Moriarty, R.W. Grosse-Kunstleve, P.D. Adams, Electronic Ligand Builder and Optimization Workbench (eLBOW): a tool for ligand coordinate and restraint generation, Acta Crystallogr. D 65 (2009) 1074–1080, https://doi.org/10.1107/S0907444909029436.

[31] P.D. Adams, P.V. Afonine, G. Bunkoczi, V.B. Chen, I.W. Davis, N. Echols, J.J. Headd, L.W. Hung, G.J. Kapral, R.W. Grosse-Kunstleve, A.J. McCoy, N.W. Moriarty, R. Oeffner, R.J. Read, D.C. Richardson, J.S. Richardson, T.C. Terwilliger, P.H. Zwart, PHENIX: a comprehensive Python-based system for macromolecular structure solution, Acta Crystallogr. D 66 (2010) 213–221, https://doi.org/10.1107/S0907444909052925.

[32] P. Emsley, K. Cowtan, Coot: model-building tools for molecular graphics, Acta Crystallogr. D Biol. Crystallogr. 60 (2004) 2126–2132, https://doi.org/10.1107/S0907444904019158.

[33] S.J. Charnock, G.J. Davies, Structure of the nucleotide-diphospho-sugar transferase, SpsA from Bacillus subtilis, in native and nucleotide-complexed forms, Biochemistry 38 (1999) 6380–6385, https://doi.org/10.1021/bi990270y.

[34] I. Just, J. Selzer, M. Wilm, C. von Eichel-Streiber, M. Mann, K. Aktories, Glucosylation of Rho proteins by Clostridium difficile toxin B, Nature 375 (1995) 500–503, https://doi.org/10.1038/375500a0.

[35] M.W. Vetting, P.A. Frantom, J.S. Blanchard, Structural and enzymatic analysis of MshA from *Corynebacterium glutamicum*: substrate-assisted catalysis, J. Biol. Chem. 283 (2008) 15834–15844, https://doi.org/10.1074/jbc.M801017200.

[36] R.A. Friesner, J.L. Banks, R.B. Murphy, T.A. Halgren, J.J. Klicic, D.T. Mainz, M.P. Repasky, E.H. Knoll, M. Shelley, J.K. Perry, D.E. Shaw, P. Francis, P.S. Shenkin, Glide: a new approach for rapid, accurate docking and scoring. 1. Method and assessment of docking accuracy, J. Med. Chem. 47 (2004) 1739–1749, https://doi.org/10.1021/jm0306430.

[37] S. Palioura, R.L. Sherrer, T.A. Steitz, D. Söll, M. Simonović, The human SepSecS-tRNA^{Sec} complex reveals the mechanism of selenocysteine formation, Science 325 (2009) 321–325, https://doi.org/10.1126/science.1173755.

[38] Y. Itoh, M.J. Brocker, S. Sekine, G. Hammond, S. Suetsugu, D. Soll, S. Yokoyama, Decameric SelA·tRNA(Sec) ring structure reveals mechanism of bacterial selenocysteine formation, Science 340 (2013) 75–78, https://doi.org/10.1126/science.1229521.

[39] K.A. Ireland, C.M. Kayrouz, J. Huang, M.R. Seyedsayamdost, K.M. Davis, Structural characterization and ligand-induced conformational changes of SenB, a Se-glycosyltransferase involved in selenoneine biosynthesis, Biochemistry 62 (2023) 3337–3342, https://doi.org/10.1021/acs.biochem.3c00452.

[40] W. Huang, J. Song, T. Sun, Y. He, X. Li, Z. Deng, F. Long, Substrate binding and catalytic mechanism of the Se-glycosyltransferase SenB in the biosynthesis of selenoneine, Nat. Commun. 15 (2024) 1659, https://doi.org/10.1038/s41467-024-46065-6.

[41] C.A. Ramirez-Mondragon, M.E. Nguyen, J. Milicaj, B.A. Hassan, F.J. Tucci, R. Muthyala, J. Gao, E.A. Taylor, Y.Y. Sham, Conserved conformational hierarchy across functionally divergent glycosyltransferases of the GT-B structural superfamily as determined from microsecond molecular dynamics, Int. J. Mol. Sci. 22 (2021), https://doi.org/10.3390/ijms22094619.

[42] P.K. Qasba, B. Ramakrishnan, E. Boeggeman, Substrate-induced conformational changes in glycosyltransferases, Trends Biochem. Sci. 30 (2005) 53–62, https://doi.org/10.1016/j.tibs.2004.11.005.

[43] L. Holm, A. Laiho, P. Törönen, M. Salgado, DALI shines a light on remote homologs: one hundred discoveries, Protein Sci. 32 (2023) e4519, https://doi.org/10.1002/pro.4519.

[44] A.R. Stampfli, K.V. Goncharenko, M. Meury, B.N. Dubey, T. Schirmer, F.P. Seebeck, An alternative active site crchitecture for O(2) activation in the ergothioneine biosynthetic EgtB from *Chloracidobacterium thermophilum*, J. Am. Chem. Soc. 141 (2019) 5275–5285, https://doi.org/10.1021/jacs.8b13023.

[45] M. Liu, Y. Yang, J.-W. Huang, L. Dai, Y. Zheng, S. Cheng, H. He, C.-C. Chen, R.-T. Guo, Structural insights into a novel nonheme iron-dependent oxygenase in selenoneine biosynthesis, Int. J. Biol. Macromol. 256 (2024) 128428, https://doi.org/10.1016/j.ijbiomac.2023.128428.

[46] H. Zhu, S.C. Peck, F. Bonnot, W.A. van der Donk, J.P. Klinman, Oxygen-18 kinetic isotope effects of nonheme iron enzymes HEPD and MPnS support iron(III) superoxide as the hydrogen abstraction species, J. Am. Chem. Soc. 137 (2015) 10448–10451, https://doi.org/10.1021/jacs.5b03907.

[47] S. Hong, K.D. Sutherlin, J. Park, E. Kwon, M.A. Siegler, E.I. Solomon, W. Nam, Crystallographic and spectroscopic characterization and reactivities of a mononuclear non-haem iron(III)-superoxo complex, Nat. Commun. 5 (2014) 5440, https://doi.org/10.1038/ncomms6440.

[48] W.A. van der Donk, C. Krebs, J.M. Bollinger Jr., Substrate activation by iron superoxo intermediates, Curr. Opin. Struct. Biol. 20 (2010) 673–683, https://doi.org/10.1016/j.sbi.2010.08.005.
[49] A. Vit, G.T. Mashabela, W. Blankenfeldt, F.P. Seebeck, Structure of the ergothioneine-biosynthesis amidohydrolase EgtC, Chembiochem 16 (2015) 1490–1496, https://doi.org/10.1002/cbic.201500168.
[50] K.V. Goncharenko, F.P. Seebeck, Conversion of a non-heme iron-dependent sulfoxide synthase into a thiol dioxygenase by a single point mutation, Chem. Commun. 52 (2016) 1945–1948, https://doi.org/10.1039/c5cc07772a.